



Intrinsic versus extrinsic seismic anisotropy: The radial anisotropy in reference Earth models

Nian Wang, Jean-Paul Montagner, Andreas Fichtner, Yann Capdeville

► To cite this version:

Nian Wang, Jean-Paul Montagner, Andreas Fichtner, Yann Capdeville. Intrinsic versus extrinsic seismic anisotropy: The radial anisotropy in reference Earth models. *Geophysical Research Letters*, 2013, 40 (16), pp.4284-4288. 10.1002/grl.50873 . insu-01399943

HAL Id: insu-01399943

<https://insu.hal.science/insu-01399943>

Submitted on 21 Nov 2016

HAL is a multi-disciplinary open access archive for the deposit and dissemination of scientific research documents, whether they are published or not. The documents may come from teaching and research institutions in France or abroad, or from public or private research centers.

L'archive ouverte pluridisciplinaire **HAL**, est destinée au dépôt et à la diffusion de documents scientifiques de niveau recherche, publiés ou non, émanant des établissements d'enseignement et de recherche français ou étrangers, des laboratoires publics ou privés.

Intrinsic versus extrinsic seismic anisotropy: The radial anisotropy in reference Earth models

Nian Wang,¹ Jean-Paul Montagner,¹ Andreas Fichtner,² and Yann Capdeville³

Received 23 June 2013; revised 6 August 2013; accepted 12 August 2013; published 28 August 2013.

[1] Seismic anisotropy usually arises from different mechanisms, which include lattice or crystallographic preferred orientation (LPO, CPO), alignment of cracks with or without fluid inclusions, fine layering, or partial melting. This makes the interpretation of anisotropy in terms of “intrinsic” (produced by LPO, CPO) versus “extrinsic” (produced by other mechanisms) properties difficult and nonunique. The radial anisotropy in the one-dimensional, global spherically symmetric reference Earth is usually claimed to be intrinsic. Here we explore whether the radial anisotropy in one-dimensional reference Earth models including preliminary reference Earth model (PREM) and the constrained reference Earth model ACY400 contains extrinsic anisotropy, especially in relation to fine layering. We conclude that as well as intrinsic anisotropy, extrinsic anisotropy introduced by finely layered models, can be considered to explain the lithospheric anisotropy in PREM, but cannot explain alone its asthenospheric anisotropy. We also find that radial anisotropy in model ACY400 is mainly intrinsic due to its petrological constraints. **Citation:** Wang, N., J.-P. Montagner, A. Fichtner, and Y. Capdeville (2013), Intrinsic versus extrinsic seismic anisotropy: The radial anisotropy in reference Earth models, *Geophys. Res. Lett.*, 40, 4284–4288, doi:10.1002/grl.50873.

1. Introduction

[2] Evidence for seismic anisotropy in the Earth’s mantle has been steadily growing over several decades. Anisotropy (azimuthal or radial anisotropy) is necessary to explain various seismological and mineralogical data, and it provides invaluable information on the geodynamics and rheology of the Earth. Anisotropy can be produced by multiple physical processes at different spatial scales λ_S (Figure 1). It exists from the microscale (crystal scale) to the macroscale, where it can be observed by seismic waves that have wavelengths λ_W up to hundreds of kilometers. Most minerals in the Earth’s upper mantle are anisotropic. Figure 1a shows a single anisotropic olivine crystal (scale $<10^{-6}$ m) [Zhang and Karato, 1995; Ben Ismail and Mainprice, 1998; Montagner, 1998], and Figure 1b shows the aggregate (e.g., peridotite) of different minerals such as orthopyroxene and clinopyroxene [Peselnick et al., 1974; Christensen

and Lundquist, 1982]. Under finite strain accumulation [Ribe, 1992], they can obtain a lattice or crystallographic preferred orientation (LPO or CPO), resulting in large-scale (>1 km) anisotropy. This can provide fundamental information on the structure and the geodynamic processes of the Earth [Hess, 1964; Peselnick et al., 1974; Christensen and Lundquist, 1982; Zhang and Karato, 1995; Ben Ismail and Mainprice, 1998; Long and Becker, 2010].

[3] At intermediate scales (10^{-3} – 10^3 m), other processes can also give rise to observed anisotropy. Cracks (with or without fluid inclusions) embedded in rocks can be aligned parallel to the main compressive stress field through the mechanism of shape-preferred orientation [O’Connell and Budiansky, 1976; Crampin, 1984; Babuska and Cara, 1991; Hudson et al., 2001] (Figure 1c), producing anisotropy when their averaged scale is much smaller than the seismic wavelength.

[4] Seismic waves are sensitive to anisotropy at even larger scales. A purely isotropic layered medium with an average layer thickness that is much smaller than the seismic wavelength will be equivalent to a vertical transversely isotropic (VTI) medium [Backus, 1962], a phenomenon called the long-wavelength equivalent effect (Figure 1d). This can occur, for example, in a laminated structure, such as sedimentary deposits with fine layers, or in a marble-cake model [Allègre and Turcotte, 1986] with superposition of various elongated strips of mantle materials. Partial melting [Kawakatsu et al., 2009] can also have a significant role in the study of seismic anisotropy. It takes place when materials of the layered Earth have different melt temperatures and reflects the geodynamics of the Earth (Figure 1e). It is mainly affected by temperature and pressure and then can be related to phase changes (for example, from solid phase to liquid phase) [see Turcotte and Schubert, 2002].

[5] Therefore, seismic anisotropy can result from LPO or CPO which is related to the strain field; or from the alignment of cracks, fine layering, or partial melting, which is related to the stress field. We classify the anisotropy produced by LPO and CPO as intrinsic anisotropy, while the anisotropy produced by other mechanisms as extrinsic anisotropy. Different mechanisms can produce anisotropy at multiple scales, making the interpretation of anisotropy difficult and nonunique [e.g., Backus, 1962; Fichtner et al., 2013]. In this paper, we consider the so-called radial anisotropy [Love, 1927; Anderson, 1961], which was made popular by preliminary reference Earth model (PREM) [Dziewonski and Anderson, 1981]. PREM is a spherically symmetric global Earth model, and it is described by density, attenuation values, and five elastic constants. The five elastic parameters, A, C, F, N, and L, are related to the velocities of horizontally and vertically propagating P waves ($A=\rho V_{PH}^2$, $C=\rho V_{PV}^2$) and transversely polarized propagating S waves ($N=\rho V_{SH}^2$,

Additional supporting information may be found in the online version of this article.

¹Institut de Physique du Globe de Paris, Paris, France.

²Department of Earth Sciences, ETH Zurich, Zurich, Switzerland.

³Laboratoire de Planétologie et de Géodynamique de Nantes, Nantes, France.

Corresponding author: N. Wang, Institut de Physique du Globe de Paris, 1 Rue Jussieu, Paris CEDEX 05 FR-75238, France. (nwang@ipgp.fr)

©2013. American Geophysical Union. All Rights Reserved.
0094-8276/13/10.1002/grl.50873

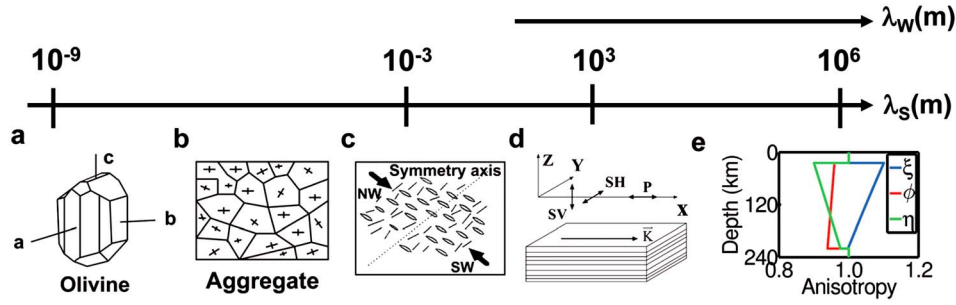


Figure 1. The existence of anisotropy from the microscale to the macroscale. (a) The anisotropic olivine crystal. (b) The anisotropic aggregate as an example of CPO. (c) Cracks filled with fluid inclusions with a symmetry axis. (d) A finely layered model that shows seismic radial anisotropy. (e) Seismic anisotropy produced by partial melting at the lithosphere and asthenosphere boundary. (f) Radial anisotropy parameters (ξ , ϕ , and η) in the top 200 km of the upper mantle of PREM. The symbols λ_s and λ_w refer to the spatial scale and the seismic wavelength, respectively.

$L = \rho V_{SV}^2$), together with three anisotropic parameters: $\xi = N/L$, $\phi = C/A$, and $\eta = F/(A - 2L)$ [Anderson, 1961]. Figure 1f shows the radial anisotropy in the top 200 km of the upper mantle of the global Earth model—PREM. The radial anisotropy (since azimuthal anisotropy is averaged out) in the one-dimensional global reference Earth models such as PREM is usually claimed to be intrinsic [Estey and Douglas, 1986; Beghein, 2010]. That is interpreted as being due to the horizontally oriented minerals (olivine) with azimuthal anisotropy averaged out, as a result of the dominant horizontal convective flow of the Earth. We propose that fine layering (related to extrinsic anisotropy) is also possible for the interpretation of the global-averaged radial anisotropy in two reference Earth models including PREM and a constrained reference Earth model—ACY400 [Montagner and Anderson, 1989].

2. The Periodic Isotropic Two-Layered (PITL) Model

[6] To explore the possibility that fine layering can explain the radial anisotropy of the reference Earth, we limit ourselves to the simplest finely layered model: the PITL model [Thomson, 1950; Postma, 1955; Anderson, 1961; Backus, 1962]. The PITL model is assumed to be periodic in the vertical direction, and it consists of alternating isotropic layered materials (Figure 2). The reason why we chose the PITL model is that we can derive its five independent parameters, to determine the unique corresponding effective vertical transversely isotropic (VTI) model that is characterized by the same number of elastic parameters.

[7] The five parameters of the PITL model are the following: the thickness proportion of the first material, defined as the fraction p_1 ; the square of the ratio of the S wave velocity to the P wave velocity of each material, θ_1 and θ_2 ; and the shear moduli of the PITL model, μ_1 and μ_2 . These effective elastic parameters connect the averaged stress and averaged strain of the long-wavelength equivalent VTI model, and their formula are detailed in Text S1 in the supporting information. For example, the parameter N , which is relevant to the transversely polarized horizontal propagating S wave velocity (V_{SH}), is given by $N = \langle \mu \rangle = p_1 \mu_1 + (1 - p_1) \mu_2$. It is the arithmetic average of the shear moduli of the PITL model over depth. The other four parameters can also be explained as algebraic combinations of the averages of the elastic parameters of the PITL model over depths.

[8] Although each layer of the PITL model is isotropic, its effective medium is anisotropic. An important consequence of this averaging is that $V_{SH} > V_{SV}$ (implies that $\xi > 1$), which is always the case for the effective model. This means that it is impossible to explain any observed anisotropy with $\xi < 1$ by using PITL models. More general cases of layered models, such as nonperiodic media, can be addressed by homogenization techniques [Allaire, 1992; Capdeville and Marigo, 2007; Capdeville et al., 2010], but this is beyond the scope of this study, which attempts to provide an analytical treatment.

3. The Stable, Long-Wavelength Equivalent Region (SLWER) Tests

[9] We now investigate whether the radial anisotropy in the upper mantle of PREM can be explained by stable PITL models. An elastic model is stable if none of the deformations have negative internal energy [Backus, 1962; Fichtner et al., 2013]. For an isotropic model to be stable, its elastic

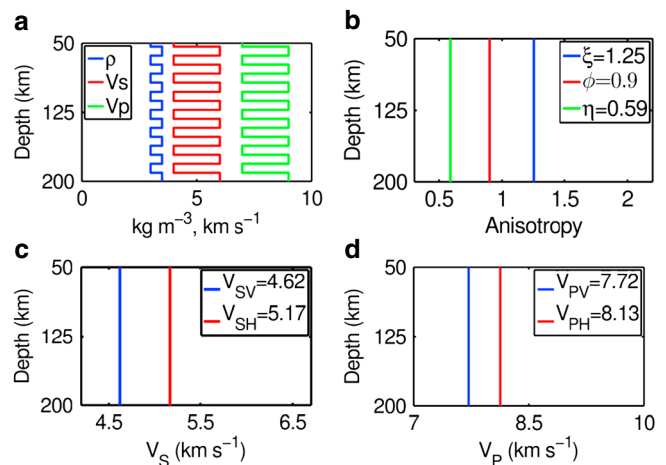


Figure 2. An example of the PITL model and its effective model showing the long-wavelength equivalent effect. (a) The densities ($\rho = 3$ and 3.5 kg m^{-3}), P wave velocities (7 and 9 km s^{-1}), and S wave velocities (4 and 6 km s^{-1}) of the PITL model with the fraction $p_1 = 0.5$. (b) The corresponding effective anisotropic parameters ξ , ϕ , and η . (c) S wave velocities V_{SV} and V_{SH} and (d) P wave velocities V_{PV} and V_{PH} of the effective model.

parameters should satisfy the conditions of $\mu \geq 0$ and $0 \leq \theta = V_S^2/V_P^2 = \mu/(\lambda + 2\mu) \leq 3/4$. Backus [1962] derived the necessary and sufficient conditions to define when a stable anisotropic model is the long-wavelength equivalent of a stable isotropic two-layered model. By parameterization of ρ , A , L , ξ , ϕ , and η , we apply these sets of conditions to the PITL model (see equations B4–B7 in Text S2) and define them as the SLWER.

[10] At each depth from the lithosphere to the asthenosphere, we use the values of ρ , L , A , and η given in PREM [Dziewonski and Anderson, 1981] (Figure 3, projections onto the ξ and ϕ plane). Figure 3 shows the possible ranges of ξ and ϕ (for anisotropic models) where there is at least a stable equivalent PITL model in blue color. The regions where it is impossible for any equivalent stable PITL model are shown in light yellow. PREM (red point) is in or close to the stable, long-wavelength equivalent region in the lithosphere, while it is further away from the stable, long-wavelength equivalent region in the asthenosphere (blue region). Therefore, extrinsic anisotropy introduced by fine layering might explain the lithospheric anisotropy in PREM, in addition to the commonly claimed intrinsic anisotropy; while the asthenospheric anisotropy cannot be explained simply by PITL models.

[11] The radial anisotropy in PREM is claimed to have an intrinsic origin (related to LPO). In other words, the higher value of V_{SH} than V_{SV} in PREM is explained by the preferentially horizontal alignment of olivine crystals that arise from plate motion of the Earth [Dziewonski and Anderson, 1981;

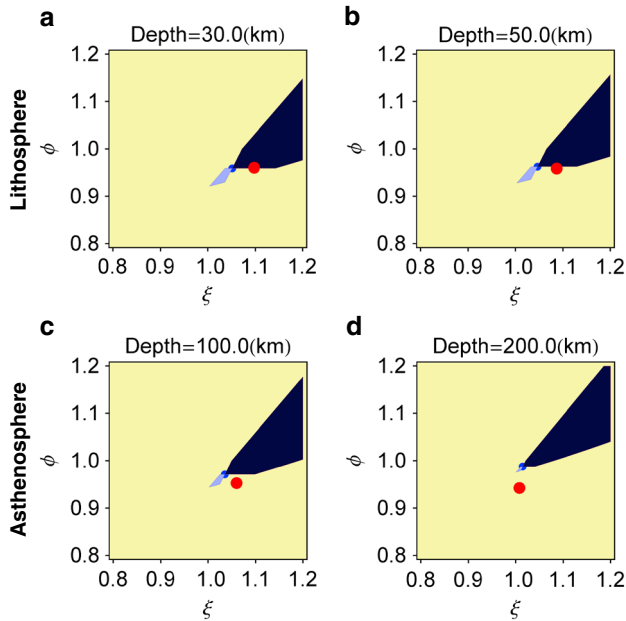


Figure 3. The stable long-wavelength equivalent region test of the radial anisotropy in the lithosphere and asthenosphere of PREM. At the depths of (a) 30, (b) 50, (c) 100, and (d) 150 km, we fix the values of ρ , L , A , and η (projections on the ξ and ϕ plane) according to the coefficients of the polynomials given in PREM. Red point, the exact location of PREM; light yellow region, the ranges where there is no equivalent PITL model; blue region, the possible ranges of the anisotropic parameters ξ and ϕ that indicate the stable, long-wavelength equivalent region: light blue region, set 1; dark blue region, set 2; blue point, set 3 (as described in the Text S2). Both ξ and ϕ vary between 0.8 and 1.2.

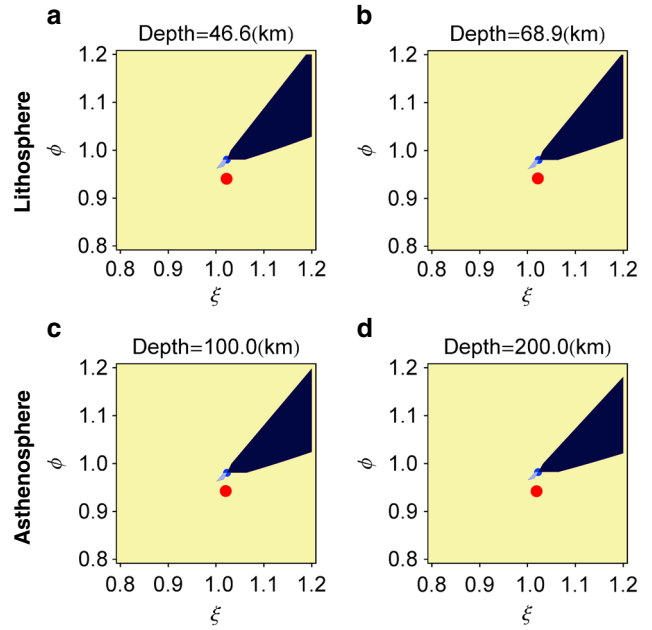


Figure 4. Same as Figure 3 but for the constrained reference Earth model ACY400 in its lithosphere and asthenosphere. At the depths of (a) 46.6, (b) 68.9, (c) 100, and (d) 200 km, we fix the values of ρ , L , A , and η given in the ACY400. Red point, exact location of the ACY400.

Ekström and Dziewonski, 1998]. At the regional scale, this appears as the surface wave azimuthal anisotropy due to the predominant horizontal deformation [Forsyth, 1975; Montagner and Tanimoto, 1991; Debayle et al., 2005]. At a global scale, PREM simply averages out the azimuthal anisotropy due to its spherical symmetry, which leads to dominant radial anisotropy (with $1 < \xi < 1.1$). The corresponding VTI model cannot be explained by simple petrological models, such as pyrolite or piclogite [Montagner and Anderson, 1989]. And the finely layered model is another solution to explain the observed anisotropy in the lithosphere (Figures 3a and 3b). In contrast, the asthenosphere is characterized by vigorous convection with small temperature heterogeneities but strong deformation, which induces large-scale LPO. So the anisotropy in the asthenosphere is probably a mixture of intrinsic and extrinsic anisotropy (may be related to partial melting) (Figures 3c and 3d).

[12] We also explore the radial anisotropy in another reference Earth model ACY400 [Montagner and Anderson, 1989]. For this model, we find that the radial anisotropy in both lithosphere and asthenosphere at all depths cannot be explained by the PITL model (Figure 4). The reason is probably that the ACY400 model uses petrological constraints that were derived from petrological mantle models, and its anisotropy, in particular, favors intrinsic anisotropy.

4. Discussion

[13] In this study, we have addressed the issue of the petrological and geodynamic interpretations of the observed seismic anisotropy. So far, LPO (related to intrinsic anisotropy) is the preferred mechanism for explaining the observed anisotropy of the Earth especially at large scale. Other mechanisms such as aligned cracks with fluid inclusions and fine layering can be considered in the crust or shallow layers of

the mantle. Partial melting [Kawakatsu *et al.*, 2009] is mainly considered in the asthenosphere where rocks are more ductile due to the high temperature and pressure conditions, but it can be also taken into account in such regions as mid-ocean ridges or in deep Earth even as deep as the inner core. The explanation of the observed seismic anisotropy is quite nonunique, because it is most of the time produced by a combination of several competing mechanisms, and a sum of intrinsic and extrinsic anisotropy. It will be very important to be able to quantify and possibly separate different effects (mechanisms of anisotropy, intrinsic versus extrinsic anisotropy) in order to avoid wrong interpretations of anisotropy. The one-dimensional global PREM has been investigated, and we have been able to partially discriminate the origins of anisotropy in its lithosphere and asthenosphere through the stable, long-wavelength equivalent region (SLWER) test. While for the constrained ACY400 model, due to the petrological constraints, its radial anisotropy is dominated by intrinsic anisotropy (almost excludes extrinsic anisotropy).

[14] To find an equivalent finely layered model such as the PITL model for PREM is not a simple question even for its lithosphere. At a depth of 30 km, we try to find an equivalent PITL model for PREM. When considering the five elastic parameters, the corresponding analytical solution is $p_1 = 0.998$ and $p_2 = 0.002$, $\mu_1 = 65.226$ GPa and $\mu_2 = 3180.457$ GPa if μ_2/μ_1 is assumed (see equations A1–A7 in Text S1), which is an unrealistic Earth model. If we just want to explain its three radial anisotropic parameters ($\xi = 1.0975$, $\phi = 0.96$, and $\eta = 0.9026$) at 30 km depth, it is possible to find equivalent PITL models. When $p_1 = 0.4$, $\rho_1 = \rho_2 = 3.3$ kg m⁻³, $V_{s1} = 4.5$ km s⁻¹ and assuming $\mu_2 > \mu_1$, we get the other parameters $V_{p1} = 8.596$ km s⁻¹, $V_{s2} = 3.288$ km s⁻¹, $V_{p2} = 6.93548$ km s⁻¹. The corresponding shear modulus contrast is $\alpha = (\mu_2/\mu_1) = 0.53$, which means a large shear modulus contrast between the two materials of the PITL. We list the equivalent PITL models for the radial anisotropy in the lithosphere of PREM in Table S1. For these equivalent PITL models, the shear modulus contrast α is between 0.5 and 0.6. Since for purely layered petrological models, the shear modulus contrast is usually larger than 0.7 [e.g., *Estey and Douglas*, 1986; *Allègre and Turcotte*, 1986], fine layering alone is unlikely to explain the lithospheric anisotropy in PREM, and intrinsic anisotropy should be invoked. For the asthenosphere of PREM, the equivalent PITL model for its radial anisotropy will be harder to find (Figure 3), and we suggest that fine layering is not a sufficient mechanism to explain the asthenospheric anisotropy in PREM compared with LPO.

[15] Though we mainly choose the simple PITL model as an example to explore whether fine layering can explain the radial anisotropy in PREM and the constrained ACY400 model, the SLWER tests can give us a hint for the key to this possibility. The structure of the Earth is more complicated, and a more complex model than the PITL model can lead to more complex effects, even in the layered case. If the model is nonperiodic or has different shapes of inclusions, we have to incorporate more degrees of freedom not just five as in the PITL model.

[16] For regional and global three-dimensional Earth, the radial anisotropy ξ below oceanic plates such as the Pacific plate and parts of the Indian Ocean is found to be as large as 10% [Ekström and Dziewonski, 1998] and the azimuthal anisotropy is relatively small (around 2%–3%) [Forsyth,

1975; *Montagner and Tanimoto*, 1991; *Debayle et al.*, 2005]. The amplitudes of the radial and azimuthal anisotropy in tomographic models were obtained from different types of data or different parameterization, making their comparison sometimes problematic. The recent tomographic upper mantle model derived by *Debayle and Ricard* [2013] from global surface wave data suggest that the amplitude of azimuthal anisotropy might have been underestimated (may be up to 4%). Also, there is a well-known discrepancy between the strength of azimuthal anisotropy inferred from surface wave models and observed shear-wave splitting (SKS) delay times [Becker *et al.*, 2012]. Therefore, to explain this discrepancy between radial and azimuthal anisotropy, the solution is nonunique and both intrinsic (LPO) and extrinsic (fine layering, partial melting) should be considered.

[17] The amplitude of azimuthal anisotropy provides strong constraints on the amplitude of radial anisotropy. For a pyrolite model, with 60% of olivine, while the rest consists of mixed pyroxenes and garnet, to explain 10% radial anisotropy, at least two thirds of olivine must be perfectly horizontally oriented, the rest being randomly oriented. The consequence is that with two thirds horizontal alignment of olivine, the corresponding amplitude of azimuthal anisotropy should be approximately 6%–8% [Montagner and Anderson, 1989] which is 2 times larger than what is usually observed. It means that the observed 10% radial anisotropy and 2% azimuthal anisotropy cannot be simply explained only by LPO, but additional mechanisms (related to extrinsic anisotropy) are required to explain this discrepancy between the radial and azimuthal anisotropy.

[18] In this paper, we propose that the observed radial anisotropy is a linear combination of intrinsic anisotropy (due to LPO), and extrinsic anisotropy especially in relation to fine layering. Extrinsic anisotropy cannot be ruled out as a possible and important contributor for explaining the anisotropy in the upper mantle. For oceanic plates, we analyze that a model with 50% intrinsic anisotropy and 50% extrinsic anisotropy can explain at the same time the observed 10% radial anisotropy and 2% azimuthal anisotropy. This model is nonunique, and a more accurate determination of this percentage must be based not only on seismological data but also on petrological constraints. We claim that fine layering plays an important role for the explanation of observed seismic anisotropy, because finely layered isotropic models can produce significant amounts of radial and even azimuthal anisotropy by tilted orientation. We hope to initiate more investigations on the possibility of fine layering that can explain both radial and azimuthal anisotropy, especially in three-dimensional crust and upper mantle models (at a regional scale), to gain a better understanding of the mechanisms of anisotropy.

[19] **Acknowledgments.** Nian Wang is supported by European I.T.N. QUEST. Andreas Fichtner was funded by The Netherlands Research Centre for Integrated Solid Earth Sciences (ISES-MD.5). Yann Capdeville is partly supported by ANR MEME (ANR-10-Blanc-613), and Jean-Paul Montagner by A.N.R. TAM and I.U.F. We thank Barbara Romanowicz and another reviewer for their helpful and constructive comments.

[20] The Editor thanks two anonymous reviewers for their assistance in evaluating this paper.

References

- Allaire, G. (1992), Homogenization and two-scale convergence, *SIAM J. Math. Anal.*, 23, 1482–1518.
- Allègre, C. J., and D. L. Turcotte (1986), Implications of a two-component marble-cake mantle, *Nature*, 323, 123–127.

- Anderson, D. L. (1961), Elastic wave propagation in layered anisotropic media, *J. Geophys. Res.*, **66**, 2953–2963.
- Babuska, V., and M. Cara (1991), *Seismic Anisotropy in the Earth*, Kluwer Academic Publishers, Boston.
- Backus, G. E. (1962), Long-wave elastic anisotropy produced by horizontal layering, *J. Geophys. Res.*, **67**, 4427–4440.
- Becker, T. W., S. Lebedev, and M. D. Long (2012), On the relationship between azimuthal anisotropy from shear wave splitting and surface wave tomography, *J. Geophys. Res.*, **117**, B01306, doi:10.1029/2011JB008705.
- Beghein, C. (2010), Radial anisotropy and prior petrological constraints: A comparative study, *J. Geophys. Res.*, **115**, B03303, doi:10.1029/2008JB005842.
- Ben Ismail, W., and D. Mainprice (1998), An olivine fabric database: An overview of upper mantle fabrics and seismic anisotropy, *Tectonophysics*, **296**, 145–157.
- Capdeville, Y., and J. J. Marigo (2007), Second order homogenization of the elastic wave equation for non-periodic layered media, *Geophys. J. Int.*, **170**, 823–838.
- Capdeville, Y., L. Guillot, and J. J. Marigo (2010), 2D nonperiodic homogenization to upscale elastic media for P-SV waves, *Geophys. J. Int.*, **182**, 903–922.
- Christensen, N. I., and S. M. Lundquist (1982), Pyroxene orientation within the upper mantle, *Geol. Soc. Am. Bull.*, **93**, 279–288.
- Crampin, S. (1984), Effective anisotropic elastic constants for wave propagation through cracked solids, *Geophys. J. R. Astron. Soc.*, **76**, 135–145.
- Debayle, E., and Y. Ricard (2013), Seismic observations of large-scale deformation at the bottom of fast-moving plates, *Phys. Earth Planet. Inter.*, **376**, 165–177.
- Debayle, E., B. L. N. Kennett, and K. Priestley (2005), Global azimuthal seismic anisotropy and the unique plate-motion deformation of Australia, *Nature*, **433**, 509–512.
- Dziewonski, A. M., and D. L. Anderson (1981), Preliminary reference Earth model, *Phys. Earth Planet. Inter.*, **25**, 297–356.
- Ekström, G., and A. M. Dziewonski (1998), The unique anisotropy of the Pacific upper mantle, *Nature*, **394**, 168–172.
- Estey, L., and B. Douglas (1986), Upper mantle anisotropy: A preliminary model, *J. Geophys. Res.*, **91**, 11,393–11,406.
- Fichtner, A., B. Kennett, and J. Trampert (2013), Separating intrinsic and apparent anisotropy, *Phys. Earth Planet. Inter.*, **219**, 11–20.
- Forsyth, D. W. (1975), The early structural evolution and anisotropy of the oceanic upper mantle, *Geophys. J. R. Astron. Soc.*, **43**, 103–162.
- Hess, H. H. (1964), Seismic anisotropy of the uppermost mantle under oceans, *Nature*, **203**, 629–631.
- Hudson, J. A., T. Pointer, and E. Liu (2001), Effective-medium theories for fluid-saturated materials with aligned cracks, *Geophys. Prospect.*, **49**, 509–522.
- Kawakatsu, H., P. Kumar, Y. Takei, M. Shinohara, T. Kanazawa, E. Araki, and K. Suyehiro (2009), Seismic evidence for sharp lithosphere-asthenosphere boundaries of oceanic plates, *Science*, **24**, 499–502.
- Long, M. D., and T. W. Becker (2010), Mantle dynamics and seismic anisotropy, *Earth Planet. Sci. Lett.*, **297**, 341–354.
- Love, A. E. H. (1927), *A Treatise on the Mathematical Theory of Elasticity*, 4th ed., Cambridge Univ. Press, Cambridge.
- Montagner, J. P. (1998), Where can seismic anisotropy be detected, *Pure Appl. Geophys.*, **151**, 223–256.
- Montagner, J. P., and D. L. Anderson (1989), Petrological constraints on seismic anisotropy, *Phys. Earth Planet. Inter.*, **54**, 82–105.
- Montagner, J. P., and T. Tanimoto (1991), Global upper mantle tomography of seismic velocities and anisotropies, *J. Geophys. Res.*, **96**, 20,337–20,351.
- O'Connell, R. J., and B. Budiansky (1976), Seismic velocities in dry and saturated cracked solids, *J. Geophys. Res.*, **81**, 2573–2576.
- Peselnick, L., A. Nicolas, and P. R. Stevenson (1974), Velocity anisotropy in a mantle peridotite from the Ivrea Zone: Application to upper mantle anisotropy, *J. Geophys. Res.*, **79**, 1175–1182.
- Postma, G. W. (1955), Wave propagation in a stratified medium, *Geophysics*, **20**, 780–806.
- Ribe, N. M. (1992), On the relation between seismic anisotropy and finite strain, *J. Geophys. Res.*, **97**, 8737–8747.
- Thomson, W. T. (1950), Transmission of elastic waves through a stratified solid medium, *J. Appl. Phys.*, **21**, 89–93.
- Turcotte, D. L., and G. Schubert (2002), *Geodynamics*, 2nd ed., Cambridge Univ. Press, Cambridge.
- Zhang, S. Q., and S. I. Karato (1995), Lattice preferred orientation of olivine aggregates deformed in simple shear, *Nature*, **375**, 774–777.